CrossMark

Label-Free Detection of Digoxin Using Localized Surface Plasmon Resonance-Based Nanobiosensor

Alireza Nikfarjam[1] · Ali Hossein Rezayan[2] · Ghasem Mohammadkhani[2] ·
Javad Mohammadnejad[2]

Abstract The scientific community finds gold nanoparticles particularly interesting due to their great applications, especially in SPR-based analysis. So far, no contributions have been made on detecting digoxin in which GNPs and LSPR technique have been used. In the present investigation, the localized surface plasmon resonance (LSPR) property of gold nanoparticles (GNPs) was utilized to develop a novel optical biosensor for the detection of digoxin. GNPs were synthesized using the sodium citrate reduction method and then made functional using the 11-mercaptoundecanoic acid (11-MUA) ligand. The carboxyl-functionalized GNPs reacted with a monoclonal antibody of digoxin through the EDC/NHS method. To characterize each processing step in the nanobiosensor preparation, UV-Vis spectrophotometry, X-ray diffraction, field emission scanning electron microscopy (FESEM), dynamic light scattering (DLS), Fourier transform infrared (FTIR), and zeta potential tests were performed. The nanobiosensor's performance was evaluated in the presence of different concentrations of digoxin in PBS and FBS. The synthesized GNPs size was estimated as 11.2 nm and present a LSPR peak at 520 nm. The size of 11-MUA-functionalized GNPs was 13.2 nm. The FTIR results revealed that 11-MUA ligand are linked to GNPs through thiol groups (Au-S-). The surface charge of 11-MUA and the monoclonal antibody-conjugated gold nanoparticles were −29.45 and −11.69, respectively. The limit of detection (LOD) of this LSPR-based nanobiosensor was 2 ng/ml. We have developed the new LSPR-based optical biosensor for direct and inexpensive detection of digoxin. This optical biosensor is easy to fabricate and the operation procedure has become more convenient.

Keywords Nanobiosensor · Localized surface plasmon resonance (LSPR) · Gold nanoparticles (GNPs) · Digoxin

Introduction

Digoxin is a cardiac glycoside and has been in use since the beginning of the twentieth century for improvement of symptoms and reduction of the hospitalization period of patients experiencing heart failure, by reducing the left ventricular ejection fraction. In addition, it is used to control supraventricular arrhythmia in patients infected with atrial fibrillation and its general effect is strengthening the muscular power of people suffering from heart failure. Digoxin has a narrow pharmaceutical range, and in case of lack of dosing and proper supervision over its use, and toxication results. One of the methods for controlling digoxin concentration in the blood serum of people is by using biosensors [1, 2].

A biosensor is a tool consisting of a bio-diagnostic element connected to a convertor [3–5]. Modern technologies tend to fabricate biosensors which can identify biological compounds, accurately and quickly. One of these sensing technologies is based on the surface plasmon resonance effect. Surface plasmon resonance sensors are based on their novel optical properties, which can sensitively and specifically measure immediate molecular interactions [6]. In this method, diagnosis is carried out directly (without intermediary) and the imaging capability is also provided [7]. Refractive index variation in the interface between the two environments with varied dielectric constants is the basic concept behind this type

✉ Ali Hossein Rezayan
ahrezayan@ut.ac.ir

[1] Department of MEMS and NEMS, Faculty of New Sciences and Technologies, University of Tehran, Tehran, Iran

[2] Department of Life Science Engineering, Faculty of New Sciences and Technologies, University of Tehran, Tehran 14399-57131, Iran

of sensor. In these two environments, a dielectric and a metal such as gold is used [8, 9].

The localized surface plasmon includes non-emission stimulation and oscillation of free electrons of metal nanostructures in the presence of an electromagnetic field [10]. According to G.Mie's theory, parameters affecting the LSPR include electrical properties, the size, and the shape of nanoparticles. According to this theory, any change in dielectric constant and refractive index causes displacement of λ_{max} (the wavelength in which a peak appeared in extinction spectrum of LSPR). This is a basis for several biosensors [11].

In recent years, GNPs have received a lot of attention due to their unique electro-optical properties like the LSPR. Another merit of the GNPs is that their LSPR properties are tuned easily by their size and shape. Consequently, the distance between the GNPs decreases, when plasmon-plasmon coupling occurs which leads to an energy loss and a shift in the absorption peak to a longer wavelength. This phenomenon happens along with a change in the color of the GNPs' solution from red to blue (blue shift) [12, 13]. It is worth noting that GNPs with various sizes can be easily synthesized and conjugated to biomolecules. Gold colloid absorbs a great deal of attention, since it is one of the most stable colloids among metallic and semiconducting particles [14]. To reach the desired electro-optical properties of the GNPs, their growth processes should be controlled exactly. To form a desirable structure, a combination of self-assembled monolayers (SAMs) and metallic colloids can be applied through a sequential deposition [15–18].

Nylander and Liedberg are the first people that used light reflection of stimulated wave of surface plasma as a sensor in 1983. Specifically, this method was used for determining the properties of thin films. In addition, this type of sensor was used as biochemical sensors [19]. Cullen used grating-based SPR systems. Since that time, a study on this type of sensors began as an alternative for the prismatic-based sensors [20]. In 1988, for the first time, the environmental sensitivity of GNPs solution was proved by Englebienne [21]. He made his biosensor based on the identification of color changes in the GNPs solution. Chilkoti et al. made a biosensor based on LSPR, using spherical GNPs with a diameter of 13.4 nm. They stabilized biotin on the GNPs to identify streptavidin. The identification limit of streptavidin in this sensor was 16 nM [22]. Endo et al. made a DNA biosensor based on LSPR. They identified DNA using GNPs with stabilized nucleic acid on them [23]. Optical biosensors based on LSPR were used for the identification of paraoxon by Lin et al. They made a paraoxon biosensor using AChE3 connected through covalent bonds to the spherical GNPs [10, 24].

Based on the aforementioned reasons and as a part of our interest in the synthesis of nanomaterials and investigation of their application in diagnosis and treatment [25–27], in the present contribution, 11-mercaptoundecanoic acid was used

to functionalize the GNPs used as digoxin biosensor in biological fluids. Little contributions were made to detect digoxin using GNPs and despite their established optical properties, this type of digoxin sensors showed acceptable detection accuracy.

Materials and Methods

Synthesis and Modification of Gold Nanoparticles

GNPs were synthesized using the Turkevich method [28, 29]. First, the glassware was soaked in Aqua Regia and left for 12 h. Then, the glassware was washed using tap water until a pH of 6 was achieved. Finally, the glassware was rinsed using Milli-Q water. In addition, 50 ml of $HAuCl_4$ (1 mM; Merck) was added to a 100-ml round bottom flask. Then a condenser was fitted to the flask, and the solution was refluxed with stirring until the solution reached its boiling point; subsequently, 5 ml of sodium citrate solution (38.8 Mm; Merck) was rapidly added to the solution under vigorous stirring. During this step, the color of the solution changed from yellow to black. The mixture was stirred for about 20 min and the color of the solution turned into wine red. Finally, the solution was allowed to cool and was kept in the dark. To determine the concentration of gold nanoparticles, UV-Vis spectrophotometry was used based on the Beer-Lambert law.

Ligand Exchange

To exchange citrate ligand with 11-mercaptoundecanoic acid on GNPs: 45 µL of 11-mercaptoundecanoic acid (11-MUA; Merck, Germany) solution (1 mM in ethanol) was added to 30 ml of the GNP so that the ratio in molarity of MUA to GNP was 120. Thereafter, the solution was mixed and left for 12 h at 4 °C. The concentration was determined the next day by UV/Vis spectrophotometry using the Beer-Lambert law [30].

Conjugation of Anti-digoxin Monoclonal Antibody to the 11-MUA-Functionalized GNPs

According to the applied studies [31], the molar ratio of antibody to GNP-11MUA must be 70. So, 84 µl of antibody (with concentration 0.5 mg/ml) was dissolved in 2 ml of sodium phosphate and incorporated to 2 ml of GNP-11MUA (C = 2 nM, pH = 7.4). This interaction was made at room temperature under vigorous stirring. After mixing the antibody and GNP-11MUA, the interaction flask was placed on the stirrer, 2 ml of sodium phosphate buffer (C = 5 mM, pH = 7) was added to the interaction flask. This connection is an electrostatic one. For covalent connection, previous stages were implemented exactly, except that instead of incorporating 2 ml of net sodium phosphate buffer, 2 ml of sodium phosphate

buffer containing (1.2 mM) NHS and (2.8 mM) EDC was added to the flask, and after proper mixing, it was kept at room temperature for 2 h. In order to remove those active carboxyl groups that are unconnected to the antibody, the final solvent was conducted with a dialysis membrane overnight in the dark conditions [31].

Interaction of Digoxin with Anti-digoxin Antibody (Ab) Immobilized on the 11-MUA-Functionalized GNPs

One milliliter of anti-digoxin antibody (Ab) immobilized on the 11-MUA-functionalized GNPs (which has been dialyzed) was poured into four different flasks and 1 ml of digoxin was incorporated softly to each one of them with concentrations of 0.2, 2, 20, and 200 ng/ml, respectively. The interaction was made at 37 °C in an incubator and digoxin was solved in PBS. The samples were left at the same temperature for 2 h to make a complete interaction. At the mentioned concentrations, an analysis of interaction between antibody connected to GNPs and digoxin dissolved in FBS was performed at the same conditions.

Results and Discussion

The sodium citrate reduction method was used to synthesize the GNPs. Thereafter, sodium citrate was substituted by the 11-MUA ligand. A monoclonal antibody of digoxin was immobilized on carboxyl-functionalized GNPs through the EDC/NHS method. The interaction of digoxin with monoclonal antibody by LSPR sensing was also investigated. Figure 1 is a schematic representation of the nanoparticles-based immunoassay.

Figure 2 shows the UV-Vis absorption spectrum of citrate-coated GNPs and 11-MUA-GNPs. Evidence from Fig. 2 shows that the absorption spectra of citrate-coated GNPs were
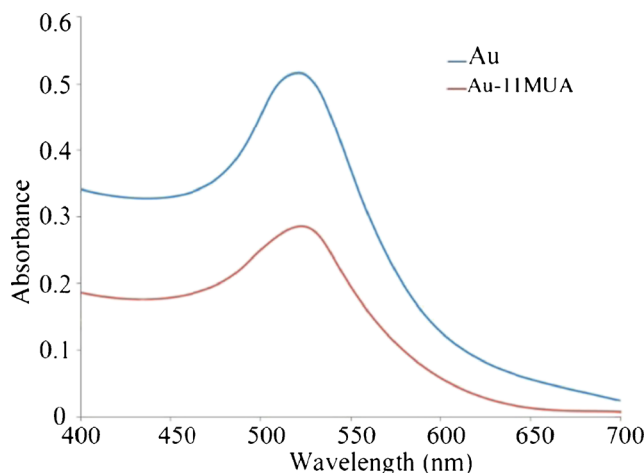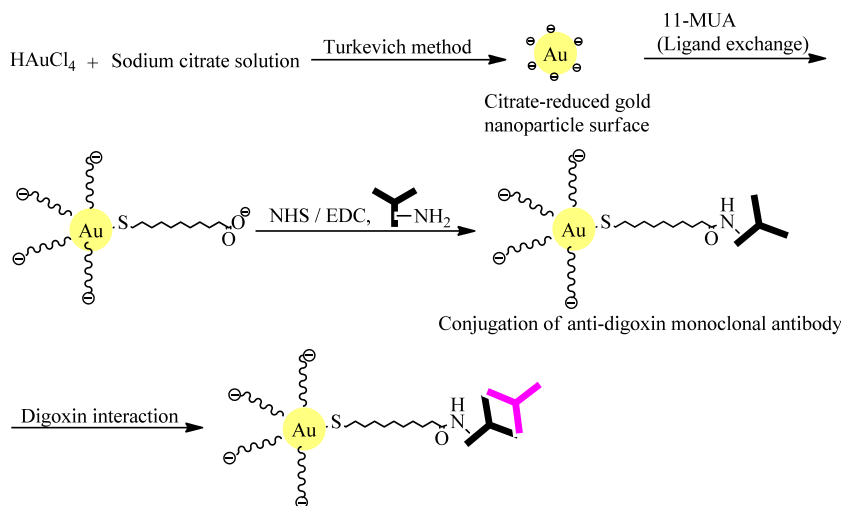

Fig. 2 UV-Vis absorption spectra of citrate-coated GNPs and 11-MUA-GNPs

maximized at 520 nm while the 11-MUA-functionalized GNPs absorption peak was maximized at 523 nm. This 3 nm increase in λ_{max} is due to variation in the dielectric constant of the environment due to the 11-MUA and may not be related to the increase in particles size; therefore, the variation range is below 20 nm (wavelength variations within this range are not subjected to particle size) [32].

Figure 3a shows the citrate-coated GNPs X-ray diffraction patterns. The specified peaks in the figure matched the reference peak (JCPDS No. 01-1174) [33]. In addition, the size of the generated GNPs was determined by the Scherrer equation. The results are summarized in Fig. 3b.

The pH stability of 11-MUA-GNPs is represented in Fig. 4a. Based on this figure, the 11-MUA-functionalized gold nanoparticles were stable for pH > 4. Figure 4b shows the stability of 11-MUA-GNPs after 12 days. After the fourth and eighth day, the absorption wavelength increased by 1 and 2 nm, respectively. Although within these 12 days, the

Fig. 1 LSPR nanobiosensor, schematic synthesis process of the antibody-conjugated 11-MUA-GNPs and the analysis of digoxin in PBS buffer and FBS
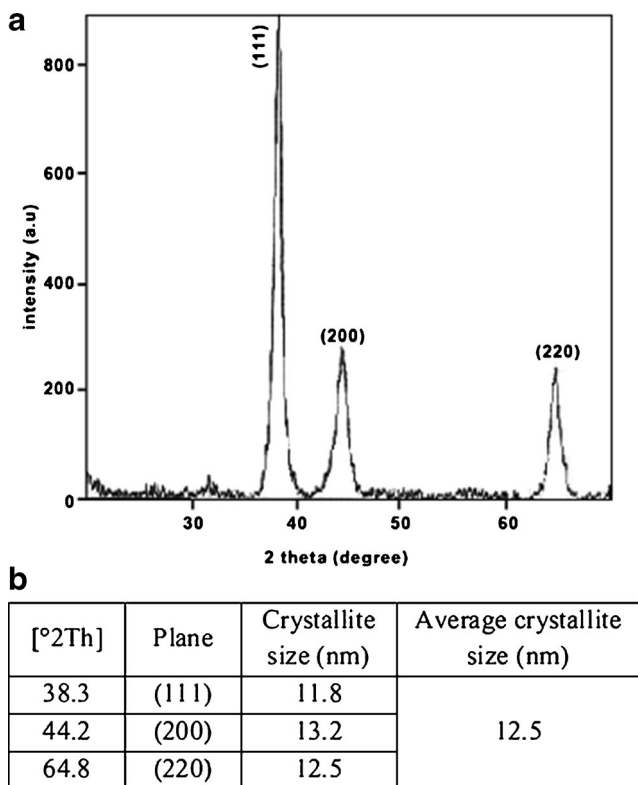
Fig. 3 a XRD pattern of citrate-coated GNPs and b Scherrer equation calculation

[°2Th]	Plane	Crystallite size (nm)	Average crystallite size (nm)
38.3	(111)	11.8	
44.2	(200)	13.2	12.5
64.8	(220)	12.5	

The FESEM of 11-MUA-functionalized GNPs, after 16 days (since the functionalized particles were synthesized), is as presented in Fig. 5c. As shown in the figure, the morphology of the nanoparticles was spherical, and the distribution of the particles was uniform. If these particles are not exposed to ultrasonic waves or any other dispersing operations, after 16 days, the size of all these particles will be about 50 nm. The presence of particles in this range of size indicates that the GNPs have been properly functionalized. The aggregation of particles shows a significant increase in size and would not be desirable. According to our results, this did not happen in the current study. The FESEM revealed that the 11-MUA-functionalized GNPs are stable enough to be used for subsequent steps. The difference in size is based on FESEM and DLS and may be related to the agglomeration of GNPs.

Figure 6 shows the FTIR spectra of (a) 11-MUA and (b) 11-MUA-functionalized GNPs. It is interesting to note that in the FTIR spectrum for the thiol group, the only useful group wavenumber for thiols is the S-H stretching vibration. On the other hand, the presence of a thiol group bound to the GNP surface through the Au–S bond was confirmed by revealing the presence of S–H groups located at the band of about 2500 cm^{-1} (Fig. 6a) and their disappearance at the same band on the Au surface (Fig. 6b), respectively. Figure 6b displays the FTIR spectrum of the 11-MUA-caped GNP sample. As specified in this figure, no bond is seen within the range of 2500–2600 (1/cm) (in free state, 11-MUA is situated in this stretching S-H bond range). This may be due to breaking of the S–H bond and formation of the Au–S bond.

Figure 7a shows the results of the UV-Vis absorption spectrum after the electrostatic and covalent immobilization of antibodies on the 11-MUA-functionalized GNPs. Generally, the λ_{max} of 11-MUA-functionalized GNPs was increased after connecting antibodies through electrostatic or covalent bonding. This is due to the increase in size and dielectric constant of the nanoparticles. In fact, a little red shift was observed which confirms that the antibodies are connected to the nanoparticles.

nanoparticles were not exposed to any dispersing operation like ultrasonic waves, as a result, the absorption wavelength increased by 4 nm only. It was concluded that the 11-MUA-functionalized gold nanoparticles have an appropriate colloid stability.

The mean size of the citrate-coated GNPs and 11-MUA-functionalized GNPs from the DLS analysis is 11.2 and 13.2 nm, respectively. The surface charge of the 11-MUA-GNPs was equal to −29.45. This value is negative due to the presence of carboxyl groups on the surface.
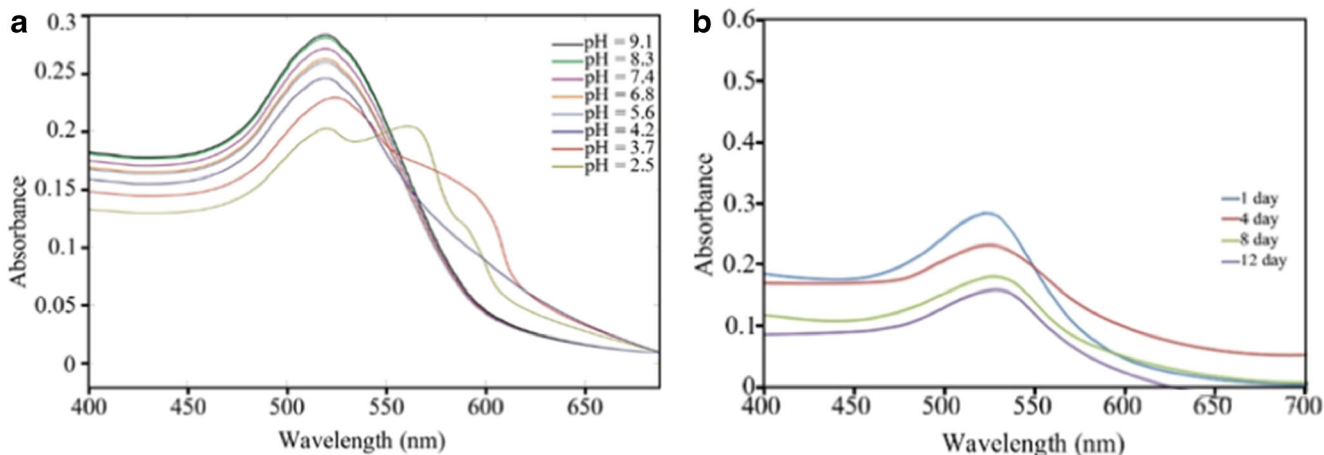

Fig. 4 UV-Vis absorption spectra of 11-MUA-GNPs at a different pH values and b various times
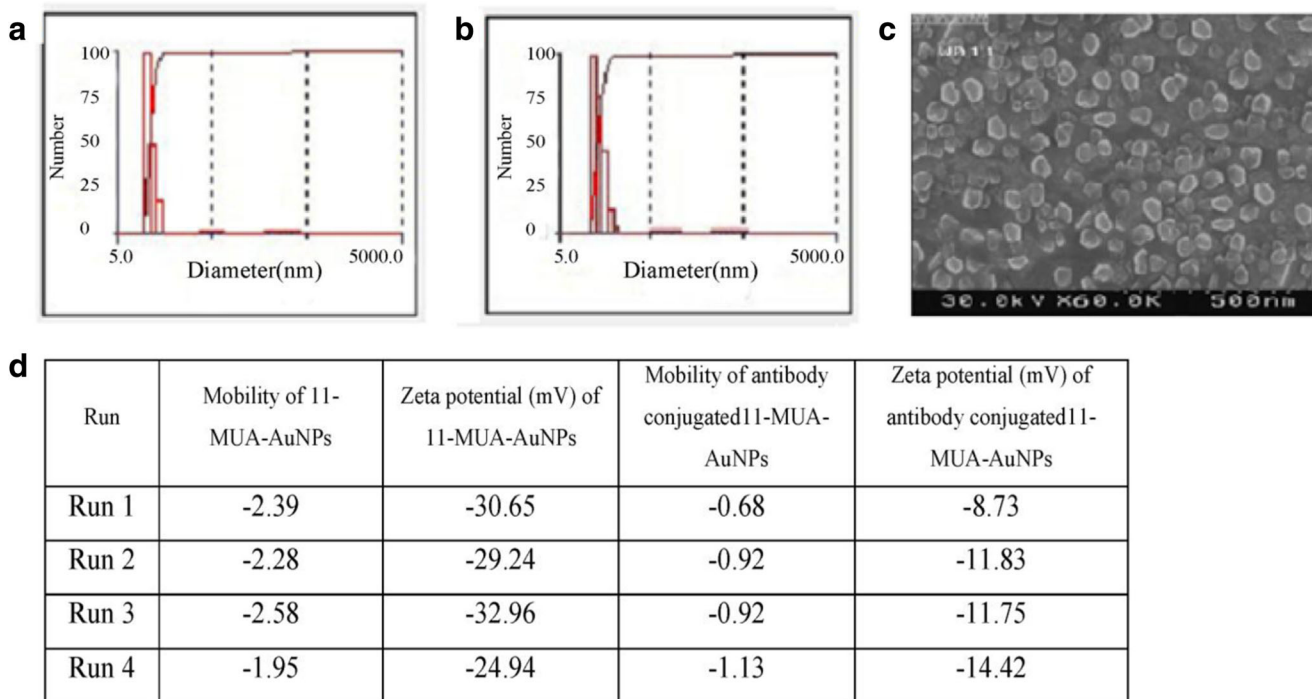
Fig. 5 **a** DLS of citrate-coated GNPs. **b** DLS of 11-MUA-GNPs. **c** FESEM images of 11-MUA-GNPs. **d** Zeta potential of 11-MUA-GNPs and antibody-conjugated 11-MUA-GNPs

Figure 7b shows the UV-Vis absorption spectra of antibody-conjugated 11-MUA-GNPs prepared in the presence of NHS/EDC at different pH values. As shown in this figure, antibody-conjugated 11-MUA-GNPs have a good stability in varied pHs; this expresses a different behavior in comparison to the 11-MUA-GNPs in Fig. 4a (before the connection of antibody to GNP-11 MUA, nanoparticles were unstable in pH less than 4).

It is interesting to note that the conjugation of antibody to 11-MUA-GNPs changes the surface charge. Figure 4d shows

the zeta potential of 11-MUA-GNPs and antibody-conjugated 11-MUA-GNPs. The mean zeta potential of the nanoparticles in this state was calculated as −11.69, which differs from the pre-connection state and became more positive (varied from −29.45 to −11.69). This may be due to the immunoglobulin which has a partial positive charge at pH of 7.4.

Figure 8 shows the UV-Vis absorption spectrum at different concentrations of digoxin interaction with antibody conjugated 11-MUA-GNPs in PBS and FBS. First, the interaction of digoxin (0.2, 2, 20, and 200 ng/ml) with antibody-conjugated 11-
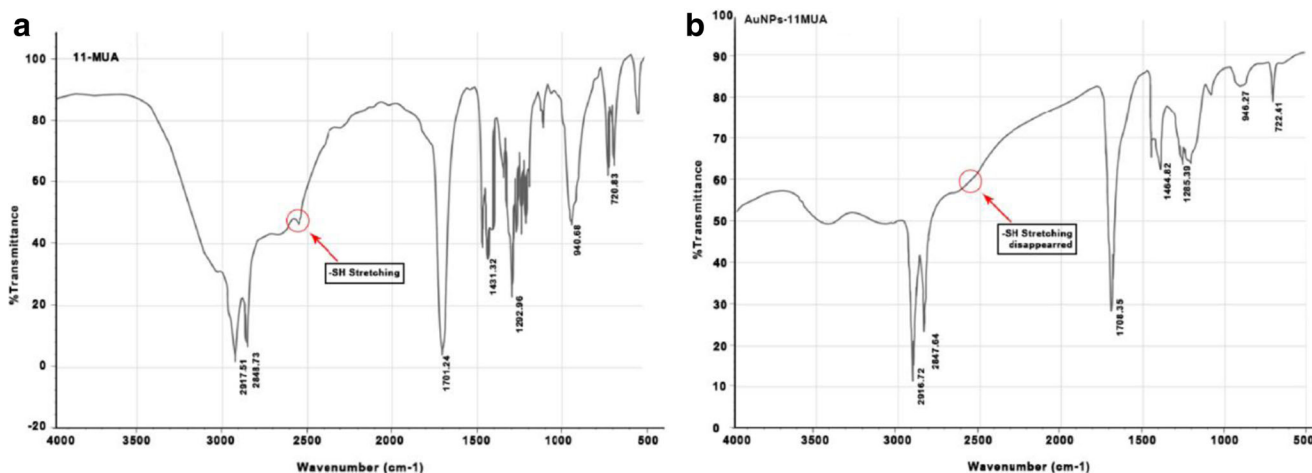

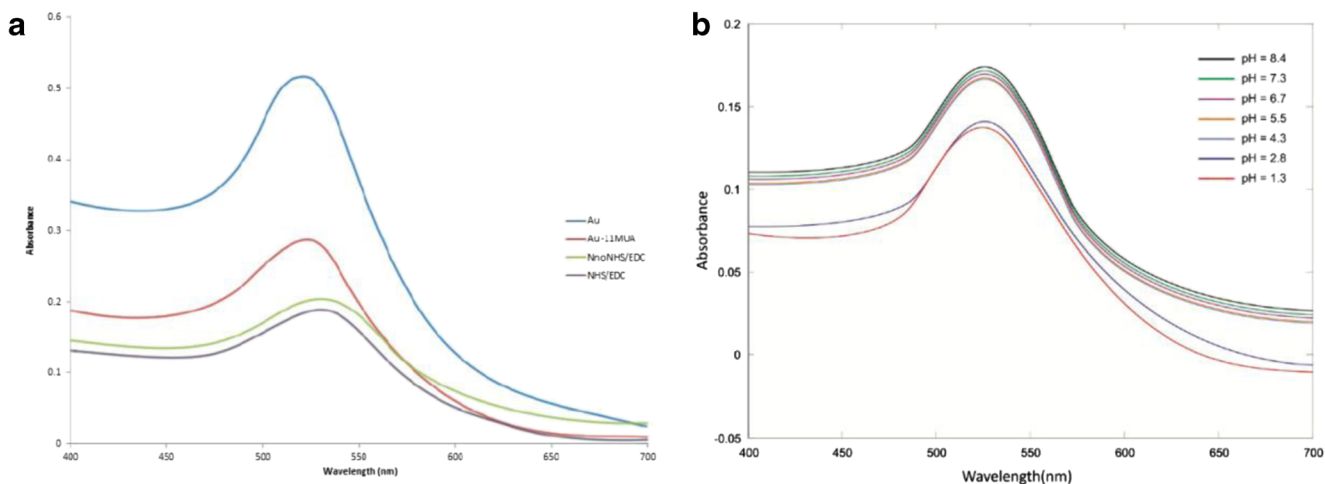Fig. 6 FTIR spectra of **a** 11-MUA and **b** 11-MUA-functionalized GNPs

Fig. 7 **a** UV-Vis absorption spectra of antibody-conjugated 11-MUA-GNPs and **b** pH effect on UV-Vis absorption spectra of antibody-conjugated 11-MUA-GNPs prepared in the presence of NHS/EDC

MUA-GNPs in PBS was measured (Fig. 8a). No significant displacement occurred for concentration of 0.2 ng/ml in λ_{max}. This means that the made biological sensor does not express any suitable response at this concentration. The λ_{max} displacement for other concentrations is significant; this confirms the interaction of digoxin with the antibody, and consequently, the identification of digoxin could be performed by this biological sensor.

The least amount of digoxin soluble in buffer, which may be identified by this biological sensor is equal to 2 ng/ml and is in the drug range of digoxin. It should be mentioned that the results are almost equal to FBS (Fig. 8b).

Figure 9 shows the sensitivity of the biosensor at different concentrations of digoxin. The sensitivity was defined as $\frac{\Delta\lambda}{\lambda_0}*100$. As shown in this figure, it is conspicuous that for
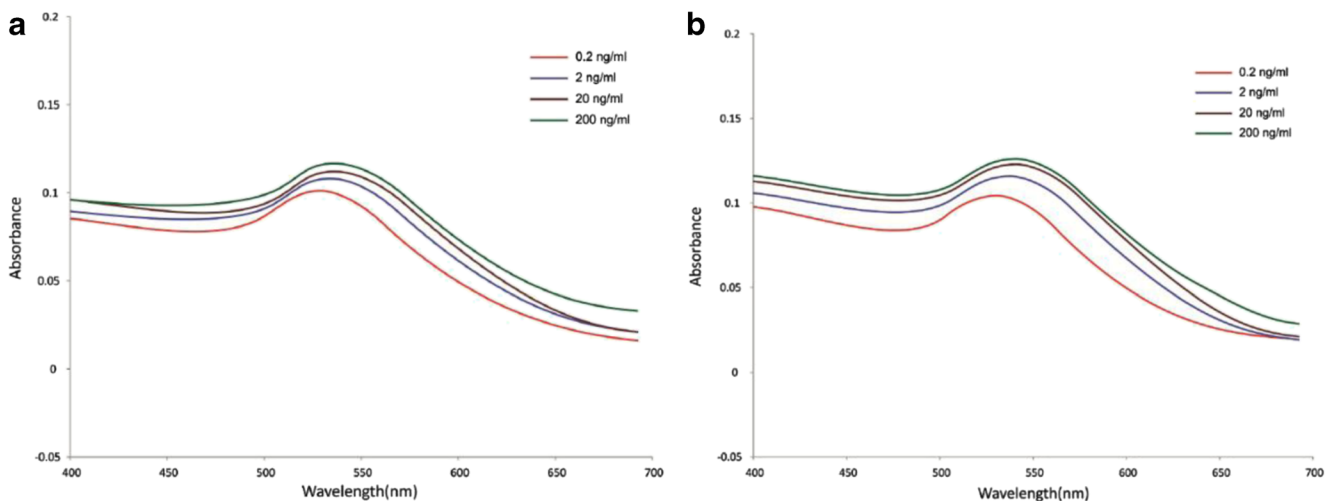
Concentration of digoxin	Absorption spectra (nm) in PBS (ng/ml)	Absorption spectra (nm) in FBS (ng/ml)
0.2	531	530
2	537	538
20	539	540
200	540	541

Fig. 8 The UV-Vis absorption spectra of different concentrations of digoxin interaction with antibody-conjugated **a** PBS buffer and 11-MUA-GNPs in **b** FBS
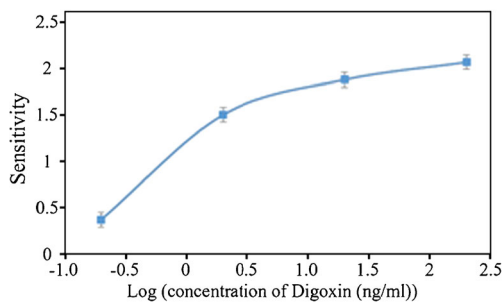
Fig. 9 Sensitivity as a function of digoxin concentration in FBS

concentrations above 2 ng/ml of digoxin, the sensitivity is high enough implying that the biosensor works properly [34].

It has to note that the limit of detection for digoxin by fluorescence quenching and colorimetric aptasensors by Emrani et al. was calculated 392 and 571 pM, respectively [35] while the limit of detection (LOD) of this LSPR-based nanobiosensor was 2 ng/ml. On the other hand, the affinity of monoclonal antibody is more than the aptamer.

It is also important to mention that the comparison of our finding with already reported paper such as [34] shows some interesting point. Our results based on LSPR label-free direct optical (UV-Vis) monitoring method while Klar et al. reported immunoassay based on competitive fluorescence quenching method via indirectly labeled hapten digoxigenin with the fluorophore Cy3B through bovine serum albumin; therefore, our designed optical biosensor is easy to fabricate and convenient in operation.

Conclusions

In this study, the functionalized GNPs were produced and used to develop a novel optical biosensor criterion to detect digoxin in biological fluids. Nanoparticles synthesized by the Turkevich method had a mean size of 11.2 nm. Based on FTIR, FESEM, DLS, and UV-Vis studies, the 11-MUA made a proper binding to the gold through its thiol (-SH end), which leads to an acceptable stability. After reacting with the monoclonal antibody of digoxin, the nanobiosensor sensitivity produced was tested using liquids with different digoxin concentrations. The limit of detection (LOD) of this LSPR-based nanobiosensor, developed in this investigation, is 2 ng/ml. This optical biosensor is easy to fabricate and the operation procedure has become more convenient. The LSPR-based label-free optical monitoring method is an ideal candidate for the future low-cost detection of diseases.

References

1. Cheng JW, Rybak I (2010) Use of digoxin for heart failure and atrial fibrillation in elderly patients. Am J Geriatr Pharmacother 8(5):419–427
2. Rich MW, McSherry F, Williford WO, Yusuf S (2001) Effect of age on mortality, hospitalizations and response to digoxin in patients with heart failure: the DIG study. J Am Coll Cardiol 38(3):806–813
3. Cooper J, Cass A (2010) Biosensors—a practical approach Oxford University Press, 2nd Edition
4. Gruson D, Homsak E (2015) Measurement of anti-Mullerian hormone: performances of a new ultrasensitive immunoassay. Clin Biochem 48(6):453–455
5. Higson S (2012) Biosensors for medical applications. Woodhead Publishing Series in Biomaterials, Cambridge
6. Reithmaier JP, Paunovic P, Kulisch W, Popov C, Petkov P (2011) Nanotechnological basis for advanced sensors. Springer Science & Business Media, The Netherlands
7. Narayanaswamy R, Wolfbeis OS (2004) Optical sensors: industrial, environmental and diagnostic applications, vol 1. Springer series on chemical sensors and biosensors
8. Liu C (2013) Localized surface plasmon resonance biosensors for real-time biomolecular binding study. Florida International University, FIU Electronic Theses and Dissertations
9. de Mol NJ, Fischer MJE (2010) Surface plasmon resonance: methods and protocols. Springer, A Product of Humana Press
10. Satija J, Bharadwaj R, Sai V, Mukherji S (2010) Emerging use of nanostructure films containing capped gold nanoparticles in biosensors. Nanotechnol Sci Appl 3:171
11. Link S, El-Sayed MA (1999) Spectral properties and relaxation dynamics of surface plasmon electronic oscillations in gold and silver nanodots and nanorods. J Phys Chem B 103(40):8410–8426
12. Shawky SM, Bald D, Azzazy HM (2010) Direct detection of unamplified hepatitis C virus RNA using unmodified gold nanoparticles. Clin Biochem 43(13):1163–1168
13. Baptista P, Eulália Pereira, Peter Eaton, Gonçalo Doria, Adelaide Miranda, Inês Gomes, Pedro Quaresma, and Ricardo Franco (2008) Gold nanoparticles for the development of clinical diagnosis methods
14. Reetz MT, Helbig W (1994) Size-selective synthesis of nanostructured transition metal clusters. J Am Chem Soc 116(16):7401–7402
15. Grabar KC, Allison KJ, Baker BE, Bright RM, Brown KR, Freeman RG, Fox AP, Keating CD, Musick MD, Natan MJ (1996) Two-dimensional arrays of colloidal gold particles: a flexible approach to macroscopic metal surfaces. Langmuir 12(10):2353–2361
16. Brust M, Bethell D, Kiely CJ, Schiffrin DJ (1998) Self-assembled gold nanoparticle thin films with nonmetallic optical and electronic properties. Langmuir 14(19):5425–5429
17. Dorogi M, Gomez J, Osifchin R, Andres R, Reifenberger R (1995) Room-temperature coulomb blockade from a self-assembled molecular nanostructure. Phys Rev B 52(12):9071
18. Kotov N (1999) Layer-by-layer self-assembly: the contribution of hydrophobic interactions. Nanostruct Mater 12(5):789–796
19. Liedberg B, Nylander C, Lunström I (1983) Surface plasmon resonance for gas detection and biosensing. Sensors Actuators 4:299–304
20. Cullen D, Brown R, Lowe C (1988) Detection of immuno-complex formation via surface plasmon resonance on gold-coated diffraction gratings. Biosensors 3(4):211–225
21. Englebienne P (1998) Use of colloidal gold surface plasmon resonance peak shift to infer affinity constants from the interactions between protein antigens and antibodies specific for single or multiple epitopes. Analyst 123(7):1599–1603

22. Nath N, Chilkoti A (2004) Label-free biosensing by surface plasmon resonance of nanoparticles on glass: optimization of nanoparticle size. Anal Chem 76(18):5370–5378

23. Endo T, Kerman K, Nagatani N, Takamura Y, Tamiya E (2005) Label-free detection of peptide nucleic acid-DNA hybridization using localized surface plasmon resonance based optical biosensor. Anal Chem 77(21):6976–6984

24. Lin T-J, Huang K-T, Liu C-Y (2006) Determination of organophosphorous pesticides by a novel biosensor based on localized surface plasmon resonance. Biosens Bioelectron 22(4):513–518

25. Nikfarjam A, Salehifar N (2015) Improvement in gas-sensing properties of TiO 2 nanofiber sensor by UV irradiation. Sensors Actuators B Chem 211:146–156

26. Hosseini M, Akbari A, Ganjali MR, Dadmehr M, Rezayan AH (2015) A novel label-free microRNA-155 detection on the basis of fluorescent silver nanoclusters. J Fluoresc 25:925–929

27. Rabiei M, Sabahi H, Rezayan AH (2016) Gallic acid-loaded montmorillonite nanostructure as a new controlled release system. Appl Clay Sci 119:236–242

28. Baptista P, Doria G, Henriques D, Pereira E, Franco R (2005) Colorimetric detection of eukaryotic gene expression with DNA-derivatized gold nanoparticles. J Biotechnol 119(2):111–117

29. Kimling J, Maier M, Okenve B, Kotaidis V, Ballot H, Plech A (2006) Turkevich method for gold nanoparticle synthesis revisited. J Phys Chem B 110(32):15700–15707

30. Haiss W, Thanh NT, Aveyard J, Fernig DG (2007) Determination of size and concentration of gold nanoparticles from UV-vis spectra. Anal Chem 79(11):4215–4221

31. Fischer MJE (2010) Amine coupling through EDC/NHS: a practical approach. In: Surface plasmon resonance. Springer, Humana Press, vol 627 of the series Methods in Molecular Biology pp 55–73

32. Lopatynskyi AM, Lopatynska OG, Guo LJ, Chegel V (2011) Localized surface plasmon resonance biosensor—Part I: theoretical study of sensitivity—extended Mie approach. Sensors Journal, IEEE 11(2):361–369

33. Xavier B, George M, Sagayaraj P (2014) Investigation on structural morphological and optical properties of gold loaded titania nanorods prepared via a novel solvothermal approach. Int J Res 1(10):1859–1864

34. Mayilo S, Ehlers B, Wunderlich M, Klar TA, Josel H-P, Heindl D, Nichtl A, Kürzinger K, Feldmann J (2009) Competitive homogeneous digoxigenin immunoassay based on fluorescence quenching by gold nanoparticles. Anal Chim Acta 646(1):119–122

35. Emrani AS, Danesh NM, Lavaee P, Jalalian SH, Ramezani M, Abnous K, Taghdisi SM (2015) Sensitive and selective detection of digoxin based on fluorescence quenching and colorimetric aptasensors. Anal Methods 7:3419–3424